ANALYTICAL MODEL OF WEAR IN UMBILICAL ARMOR WIRES
OMAE, Houston, 1994

Warren T. Jones
Consultant
Katy, Texas

William P. Stewart
Stewart Technology Associates
Houston, Texas

ABSTRACT

Bending stresses in the armor wires of a well-designed umbilical cable are usually well below the endurance limit of the wire material, so fatigue should not be a problem. However, with each bending cycle, the armor wires slip with respect to each other. The possibility exists that the resulting wear and reduction in wire cross section area could eventually lead to fatigue crack initiation and failure. Because the armor wires are of circular cross section, if a wire in the outer armor layer moves far enough with respect to a wire in the inner armor layer, contact is lost, and no wear can occur. Methods are developed for calculating the distance for which the wires are in contact during a single bending cycle and the depth of wear produced by a number of constant bending cycles using Archard's Law of Wear. This procedure is extended to calculate total depth of wear caused by a series of environmental loadings on the umbilical, each of which results in a different bending curvature of the umbilical. This extension allows calculation of total wear and effect on fatigue initiation over the umbilical service life. Predictions of the method agree with results of a qualifying test on an umbilical; however, additional testing is required to better define characteristics of this type of wear — particularly the wear coefficient for this combination of armor wire geometry and material.

INTRODUCTION

Bending stresses in the armor wires of a well-designed umbilical cable are usually well below the endurance limit of the wire material, so fatigue of the wires should not be a problem over the service life of the umbilical. However, with each bending cycle of sufficient amplitude, the armor wires slip with respect to each other. The possibility exists that the resulting wear and reduction in wire cross section area could eventually lead to fatigue crack initiation and failure.

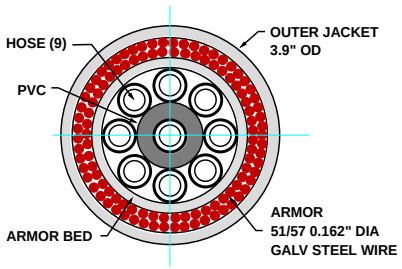

FIGURE 1 UMBILICAL CROSS-SECTION

An umbilical cable, shown in Figure 1, designed by Multiflex for installation in deep water, was to be qualified by imposing a limited number of bending cycles on a specimen subjected to a constant tension. Calculated values of armor wire bending stress were well below the endurance limit of the armor wire material; therefore, observable fatigue damage was not expected for the 50,000-cycle qualifying test. Wear was expected to be the only result of the test, so a method of calculating wear during the test was required.

In addition, prediction of wear during the umbilical service life was required in order to estimate the effect of wear on fatigue. To this end, finite element analyses of the umbilical suspended between a semi-submersible platform and the sea floor were

conducted for the expected environmental conditions during the service life. The usual method of dividing wave data represented by a scatter table of wave height, period, and direction into discrete wave height/period load cases was followed. A more detailed description of this methodology is given in Claydon et al. (1992). The result was a table of load cases and their corresponding values of maximum bending curvature, which occurred at the top of the umbilical.

Adhesive wear caused by two solids rubbing on each other is described by an equation commonly known as Archard's Law:

$$V = k\frac{F_c\, L}{H} \tag{1}$$

where V is the volume of material removed from the softer of the two solids, k is a wear coefficient, F_C is the contact force between the two wearing surfaces, L is the total relative contact distance, and H is the indentation hardness of the softer of the two solids (Archard, 1953, Chang, 1987, Rabinowicz, 1980). Archard (1980) points out that division of both sides of this equation by the area of contact gives a depth of wear in terms of a contact pressure, and the resulting equation has been used in calculations of wear in unbonded flexible pipe armor wires which have a rectangular cross-section (Claydon et al. 1992, Estrier, 1992, Feret et al., 1986, Nielsen et al., 1990).

Recent literature on wire ropes and armored power cables has described the mechanics of the armor wires and investigated fatigue (e.g., Casey and Lee, 1989, Knapp and Chiu, 1988, Llorca et al., 1989, Raoof, 1993). Only Velinsky and Schmidt (1988) consider wear in a cable type of structure, but their concern is the effect of wear on cable properties (axial stiffness, in particular), rather than the prediction of wear.

The following section presents approximate equations describing the mechanics of the armor wires. Because the armor wires are of circular cross section, if a wire in the outer armor layer moves far enough with respect to a wire in the inner armor layer, contact is lost, and no wear can occur. Calculation of the distance for which the wires are in contact during a single bending cycle is described, followed by the development of a method based on Archard's Law to calculate the depth of wear for a number of constant bending cycles. This procedure is next extended to calculate total depth of wear caused by the complete series of load cases, each resulting in a different, constant, bending curvature, allowing a estimation of total wear and effect on fatigue over the umbilical service life. The paper concludes with a comparison of predictions with results of the qualifying test and the implications for the predicted service life.

ARMOR WIRE MECHANICS

The following equations represent engineering approximations rather than exact expressions of the non-linear response of armor wires to bending and stretching of a cable type of structure. They have the great advantage of relative simplicity, and a past history of being able to produce useful results when judiciously applied.

For a straight section of umbilical cable under no load, the armor wires have a helical configuration. For the coordinate system shown in Figure 2, the parametric form of the helical configuration is given below.

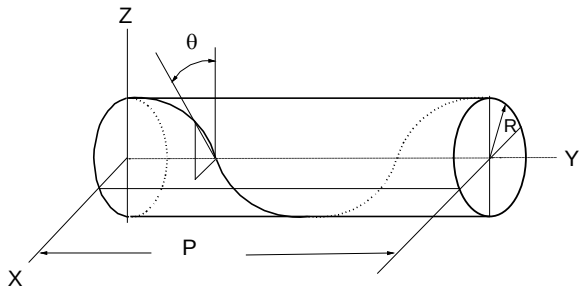

FI

GURE 2 Helix Geometry

$$x = R\sin\theta \tag{2}$$

$$y = \frac{R}{\tan\alpha}\theta \tag{3}$$

$$z = R\cos\theta \tag{4}$$

where R is the radius of the helix, θ is the parametric angle, and α, the lay angle, is defined as the angle between the helical armor wire and the y axis.

If a straight section of umbilical is loaded by an axial tension, the stress in each individual armor wire is given by (Berge and Olufsen, 1992)

$$\sigma_a = \frac{T_w}{nA\cos\alpha} \tag{5}$$

where T_W is the tension in the umbilical, n is the number of armor wires, A is the cross sectional area of an armor wire, and α is the armor wire lay angle.

When the umbilical (the cylinder in Figure 2) is uniformly bent in the y-z plane , the helix now is formed on the surface of a torus. The radius of the torus is the bend radius of curvature, ρ, and its reciprocal is the curvature, κ, of the bent umbilical.

As the umbilical is gradually bent, the helix is held to the surface of the torus by friction. When the curvature reaches a certain critical value, friction is overcome, and the helix slips on the surface of the torus. Feret and Bournazel (1987) assume that the helix moves into a geodesic curve on the surface of the torus. Witz and Tan (1992) assume that a point on the helix slips along the tangent to helix.

Feret and Bournazel (1987) give the stress in an armor wire due to the curvature, κ, of the umbilical as

$$\sigma_b = Er\kappa\cos^2\alpha\frac{\cos\theta}{1+R\kappa\cos\theta} \tag{6}$$

where E is Young's modulus for the armor wire material, and r is the armor wire radius. Note that the wire bending stress is a maximum at θ = 0, that is, at the location of maximum bending stress in a solid circular bar of radius R bent to a curvature κ. This expression is based on the armor wire taking the geodesic shape on the bent torus.

Witz and Tan (1992) provide an alternate expression for the bending stress in an armor wire based on tangential sliding of the helix

$$\sigma_b = Er\kappa(1+\sin^2\alpha)\cos\alpha\cos\theta \tag{7}$$

Estrier (1992) gives the following expression for the critical curvature at which slip begins to occur between an armor layer and its underlying core or layer.

$$\kappa_c = \frac{\pi^2 P_c f}{8Er\sin\alpha\cos^2\alpha} \tag{8}$$

where P_c is the contact pressure between the armor layers caused primarily by the axial tension load on the umbilical. (For submerged umbilicals, the effects of internal and external pressure also contribute), and f is the coefficient of friction between the slipping layers

The contact pressure between the inner armor wire layer and an underlying pressure layer (the armor bed in Figure 1) is given by Feret and Bournazel (1987). Feret et al. (1986) state that the contact pressure between two tension layers is about equal to half this value. Knapp and Chiu (1988) provide a derivation of contact pressure between two armor wire layers and arrive at the same basic expression as Feret. The difference is that Knapp and Chiu have a multiplying factor of n/(n+m) instead of 1/2. Here, n is the number of wires in one layer, and m is the number of wires in the adjacent layer. Because the number of wires in a layer does not vary *greatly* from one layer to the next, this factor is always approximately equal to 1/2. The resulting expression is

$$P_c = \frac{T_m \tan^2\alpha}{4\pi R^2} \tag{9}$$

where T_m is the mean, axial tension in the umbilical.

As the umbilical is bent and its curvature exceeds the critical curvature given by Equation (8), the armor layers slip on the surface of the torus. Feret et al. (1986, 1987) and Witz and Tan (1992) make different assumptions about the direction of this slip. Berge and Olufsen (1992) point out that the assumption of the geodesic curve does not seem to give correct prediction of the hysteric bending behavior; and that better predictions are obtained by assuming only longitudinal slip along the tangent to the armor wire axis. Further developments here are based on the axial slip assumption of Witz and Tan (1992).

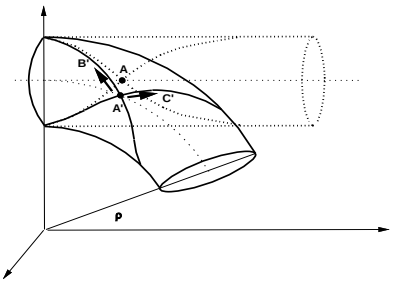

FIGURE 3 AXIAL SLIP DIRECTIONS

Figure 3 illustrates schematically the nature of the armor wire axial slippage. Dotted lines show the straight umbilical with 2 armor wires of opposite lay in contact at Point A. When the umbilical is bent and the wires do not slip, Point A moves to Point A'. This is shown in Figure 3 with solid lines. Axial strain in each wire is not constant along its length in this no-slip condition, so when friction is overcome, the wires slip along their own tangents to redistribute the axial strain. The motion is such that tensile strains are reduced and compressive strains are increased (toward zero). Portions of the wires above the bend neutral axis develop tensile strains. Hence the motion in the right-hand lay wire is from Point A' toward Point B'. Similarly, the motion in the left-hand lay wire is from Point A' toward Point C'.

Tan et al. (1991) give the maximum slip of a wire along its own tangent, which occurs at Point A in Figure 3, as

$$\delta = R^2\kappa\frac{\cos^2\alpha}{\sin\alpha} \tag{10}$$

This agrees with the expression for the tangential component of slip given by Ferret et al. (1987). Note that Ferret et al. also have a component of slip perpendicular to the tangential direction in order to reach the geodesic configuration.

CONTACT DISTANCE

Consider that some wear between armor layers has already occurred, and develop the surface of contact onto a plane. The result is shown in Figure 4. The dark diamonds, labeled "No-Motion Contact Area," represent the contact area between flats worn on two wires when the umbilical is straight. Point A, located in the central diamond, is the same Point A of Figure 3 where two wires cross the neutral axis of the umbilical. As the umbilical bends, the wires slip, changing the location of the areas in contact. Around the central diamond, the contact areas on each of the top and bottom wires during a bend cycle are indicated by cross-hatched areas.

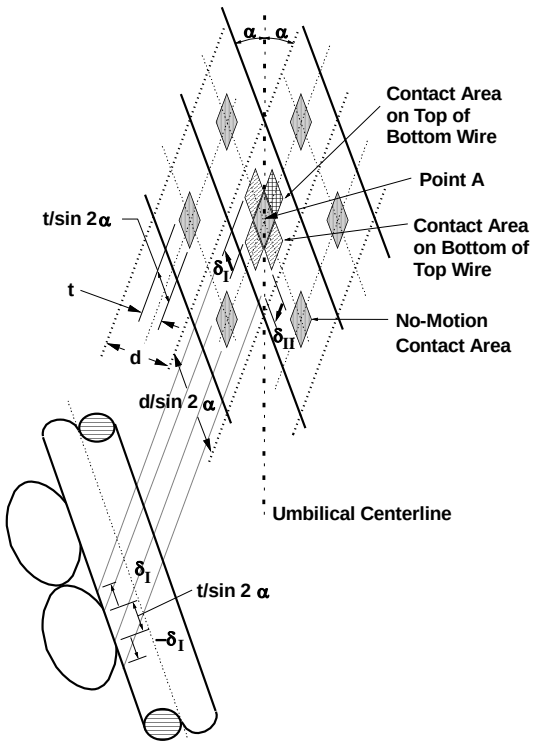

FIGURE 4 WEAR PATTERN

At the bottom Left of Figure 4, a section through the top wire centerline is shown, with the bottom wires seen as elliptical sections. During a bending cycle, every point of the top wire moves an amount δ_I to the left, an amount δ_I back to the original position, an amount δ_I to the right (indicated as $-\delta_I$), and an amount δ_I back to the original position. At the same time, the bottom wire moves in the same manner along its own axis with amplitude δ_{II}. The result is that as wear takes place, the extensions to the No-Motion Contact Area are formed as shown around the central diamond and Point A in the figure.

Consider only the motion of the top wire in order to define the contact (wear) surface on the bottom of the top wire. The top part of Figure 5(a) is the section through the top wire shown in Figure 4. Wear is just beginning, so the flat, or chord, t, on the bottom wire is less than the slip δ_I of the top wire, that is, $0 \le t/\sin 2\alpha < \delta$. The motion of Point a, which is located on the top wire adjacent to the bottom wire chord extremity, is indicated in the figure.

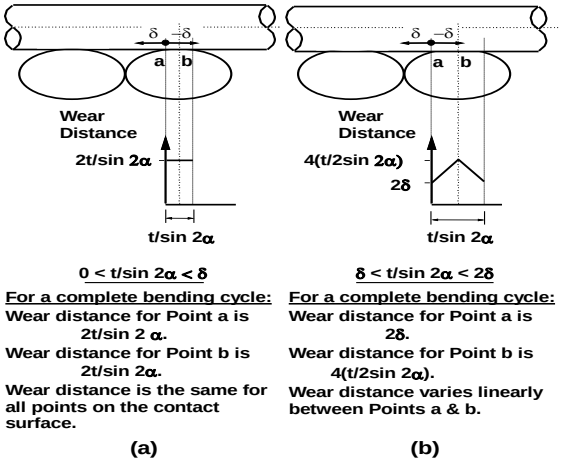

FIGURE 5 CONTACT DISTANCE

As Point a moves to the left an amount δ and back to its original position, there is no contact with the bottom wire. As it moves to the right an amount δ and back to its original position, the total contact distance is twice the projection of the bottom wire chord into this plane, or $2t/\sin 2\alpha$. Point b, located originally adjacent to the centerline of the bottom wire has the same contact distance for a bending cycle, and in fact every point on the top wire which is in contact with the bottom wire chord in the No-Motion position has this same contact distance. This is shown in the plot of Wear Distance as a function of position in the bottom portion of Figure 5(a). The average wear distance, $\overline{w}$, for every point is the area under the curve divided by $t/\sin 2\alpha$, or $2t/\sin 2\alpha$.

As further wear occurs, the chord length t increases so that $t/\sin 2\alpha$ becomes greater than the slip distance δ. This situation is shown, and development of the Wear Distance curve is explained in Figure 5(b). Again, the average wear distance, $\overline{w}$, is the area under the curve divided by $t/\sin 2\alpha$.

As still further wear occurs so that $t/\sin 2\alpha$ becomes greater than twice the slip distance δ, the shape of the Wear Distance curve changes again as shown in Figure 6(a). No further change in shape occurs until much of the bottom wire has worn away so that the gap, G, between the wires becomes so small that Point a in Figure 6(b) contacts and slides over the adjacent wire. Of course, as further wear occurs, the gap distance G decreases. From Figure 4, the gap between the wires, G, is easily seen to be

$$G = 2\left[\frac{d/2}{\sin 2\alpha} - \frac{t/2}{\sin 2\alpha}\right] \tag{11}$$

This analysis does not continue past the point where the gap G is reduced to zero, i. e., half of the wire is worn away.

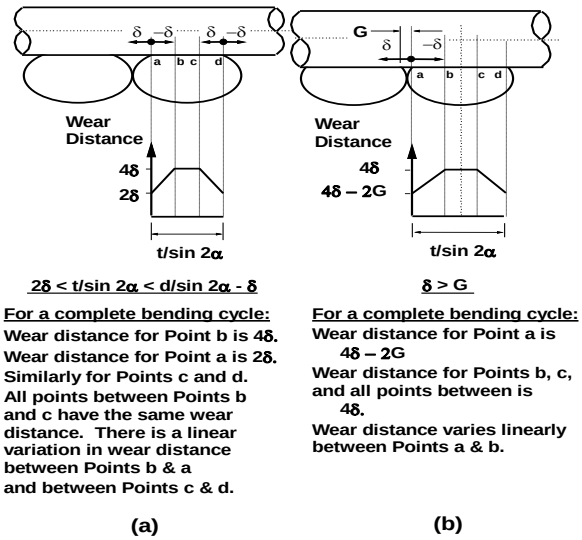

FIGURE 6 CONTACT DISTANCE

If the top and bottom wires were in contact throughout a complete bending cycle, then the total contact distance would be equal to 4δ. Each of the average wear distances, calculated as the average of the Wear Distance curves shown in Figures 5 and 6, may be manipulated into the following form

$$\bar{w} = 4\delta\zeta \tag{12}$$

where ζ is a non-dimensional factor If t and δ are non-dimensionalized by the wire diameter d, and (^) represents a non-dimensionalized ( ), the various regions and corresponding values of ζ are as follows:

$$0 \le \frac{\hat{t}}{\sin 2\alpha} < \hat{\delta}, \quad \zeta = \frac{\hat{t}}{2\hat{\delta}\sin 2\alpha} \tag{13}$$

$$\hat{\delta} \le \frac{\hat{t}}{\sin 2\alpha} < 2\hat{\delta}, \qquad \zeta = \frac{1}{4}\left(1 + \frac{\hat{t}}{\hat{\delta}\sin 2\alpha}\right) \tag{14}$$

$$2\hat{\delta} \le \frac{\hat{t}}{\sin 2\alpha} < \frac{1}{\sin 2\alpha} - \hat{\delta}, \qquad \zeta = 1 - \frac{\hat{\delta}\sin 2\alpha}{2\hat{t}} \tag{15}$$

$$\frac{1}{\sin 2\alpha} - \hat{\delta} \le \frac{\hat{t}}{\sin 2\alpha} \le \frac{1}{\sin 2\alpha}, \qquad \zeta = 1 - \frac{1 - \hat{t}}{2\hat{t}} \tag{16}$$

These equations are plotted in Fig 7 for several values of $\hat{\delta}$.

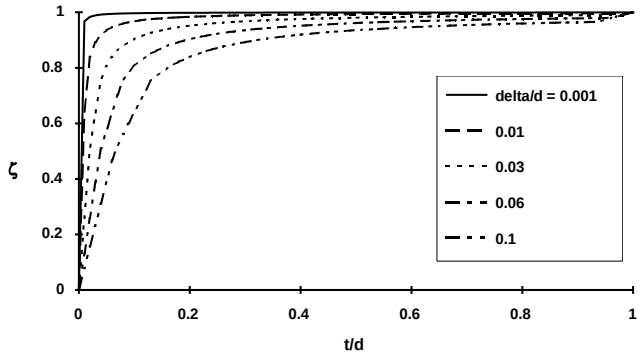

FIGURE 7 NON-DIMENSIONAL WEAR FACTOR

Wear volume is based on total distance one body has traveled over another. Everything so far has been concerned only with the distance traveled by a point on the top wire, but the bottom wire is also moving during the bending cycle. Consider two points, one on the top wire and one on the bottom wire, which are initially in contact. The point on the top wire moves a distance δ_I along its tangent during bending of the umbilical, and the point on the bottom wire moves a distance δ_{II} along its tangent. The relative slip between these two points over one-quarter of a bending cycle is given by Δ, and is calculated as a vector difference as shown in Figure 8. If the difference in torus radius, R, of the two armor wire layers is neglected, then δ_I and δ_{II} both have the same value; calling that value δ, the magnitude of the total relative slip is

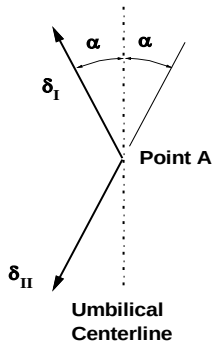

$$\underset{\sim}{\Delta} = [-\delta_I \sin(\alpha) + \delta_{II}\sin(\alpha)]\,\underset{\sim}{i} + [\delta_I \cos(\alpha) + \delta_{II}\cos(\alpha)]\,\underset{\sim}{j}$$

FIGURE 8 RELATIVE SLIP

$$\Delta = 2\delta\cos\alpha \tag{17}$$

In order to calculate the total relative distance over which the top and bottom wires are in contact, and therefore wearing, the same analysis leading to Equation (17) is repeated using the

average wear distance $\overline{w}$ instead of δ. The result is that the total relative wear distance over a complete bending cycle is given by

$$\Delta_w = 2\overline{w}\cos\alpha \tag{18}$$

WEAR CROSS-SECTION

Consider a number of bending cycles having a constant amplitude of curvature. The distance L in Archard's Law, Equation (1), is taken to be the relative wear distance Δ_w, and for more than a single bending cycle,

$$L = \Delta_{w_1} + \Delta_{w_2} + \Delta_{w_3} + \ldots \Delta_{w_N} \tag{19}$$

where N is the number of cycles and Δ_w is the contact distance per cycle give by Equation (18). Multiply the right hand side of Equation (1) by N/N and observe that L/N is the average relative contact distance per cycle. Using Equations (18) and (12), the average relative contact distance, and hence L/N, may be expressed as

$$\frac{L}{N} = 2\cos\alpha\ (4\ \delta)\overline{\zeta} \tag{20}$$

where $\overline{\zeta}$ represents the average value of ζ. Let $\hat{t}_f$ represent the final value of the non-dimensional chord distance $\hat{t}$ after N cycles; then this average value of $\overline{\zeta}$ is given by

$$\overline{\zeta} = \frac{1}{\hat{t}_f}\int_0^{\hat{t}_f} \zeta\, d\hat{t} \tag{21}$$

Archard's Law, Equation (1), becomes

$$V = \frac{8kF_c N\delta\ \cos\alpha}{H}\overline{\zeta} \tag{22}$$

Equations (21) and (22) are the desired equations for the wear volume in terms of the final chord distance t. But cross-sectional wear, rather than volume, is of concern.

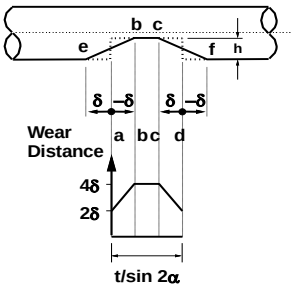

Wear depth will be greatest between Points b & c.
Wear depth will be zero at Points e & f, the extremities of contact.

FIGURE 9 CONTACT LENGTH

The volume of material that is worn off the top armor wire is distributed over some distance along the wire. Figure 9 is a greatly exaggerated view of the wear along the top wire for the condition shown in Figure 6(a). Between Points b and c, the wear depth should be constant at some value h. The variation in depth between Points b and e is not known exactly, but *if* it is linear as shown, then the volume of the worn-away trapezoid is merely the depth, h, times the distance ad, which is t/sin 2α. That is, cross sectional wear area can be obtained by dividing the volume of material worn away by t/sin 2α.

When this distance is divided into the wear volume, Equation (22), the following expression for the cross-sectional wear area is obtained:

$$A_w = \frac{8kF_c N\hat{\delta}\cos\alpha\ \sin 2\alpha}{H}\frac{\overline{\zeta}}{\hat{t}_f} \tag{23}$$

where the hat (^) over δ indicates that it has been non-dimensionalized by dividing by the armor wire diameter, d.

For a circular cross-section wire, this area is taken to be in the shape of a segment of a circle as shown in Figure 10. Final chord distance t_f is indicated there, along with the dimension h which is a readily measurable depth-of-wear dimension. In terms of $\hat{t}_f$, the segment area is given by

$$A_{seg} = r^2\left[\cos^{-1}\sqrt{1-\hat{t}_f^2} - \hat{t}_f\sqrt{1-\hat{t}_f^2}\right] \tag{24}$$

Equations (23) and (24) may now be equated and solved iteratively for $\hat{t}_f$, the final wear chord length, remembering that the average ζ, Equation (21), involves one or more of Equations depending on the value of $\hat{t}_f$.

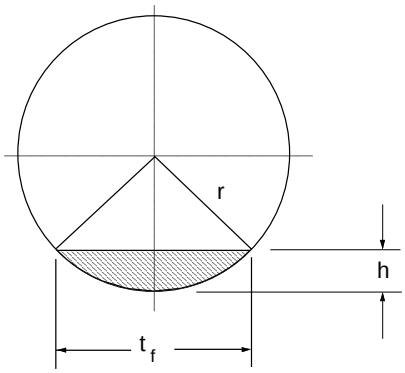

FIGURE 10 WEAR OF ARMOR WIRE

For convenience, define the following non-dimensional constant, γ, which contains properties of the umbilical, the armor wire material, and the contact load, F_C, which is constant since the mean tension in the umbilical is constant throughout the N cycles of bending.

$$\gamma = \frac{8kF_c \cos\alpha \sin 2\alpha}{H r^2} \tag{25}$$

Equating Equations (23) and (24) now results in the following transcendental equation for the determination of $\hat{t}_f$.

$$\gamma N\hat{\delta} I(\hat{t}_f) = \hat{t}_f^2\left[\cos^{-1}\sqrt{1 - \hat{t}_f^2} - \hat{t}_f\sqrt{1 - \hat{t}_f^2}\right] \tag{26}$$

where

$$I(\hat{t}_f) = \int_0^{\hat{t}_f} \zeta \, d\hat{t} \tag{27}$$

Closed-form evaluations of these integrals are provided in the Appendix for use in the iterative solution of Equation (**Error! Bookmark not defined.**).

EXTENSION TO CALCULATION OF SERVICE LIFE

Although the equations appear complicated, the solution for bending cycles of constant curvature described above is straightforward. When several load cases are considered, further assumptions are required regarding the order of wear. Each load case contains N_i waves (cycles) which occur over the service life of the umbilical, and each load case causes a certain umbilical curvature κ_i resulting in a certain δ_i. The volume of wear for this load case is given by Equation (22) as

$$V_i = \frac{8kF_c \cos\alpha}{H} N_i \delta_i \bar{\zeta}_i \tag{28}$$

Here, the assumption has been made that the mean umbilical tension, and therefore the contact force, is the same for each load case; therfore, F_c is not subscripted.

Now assumptions must be made as to how the wear due to load case i occurs in relation to the wear due to some other load case j. In reality, all waves which have been grouped into one particular load case do not occur first, followed by all waves of a second load case, and so on. However, short of a program to simulate changing wave conditions over the course of a year, some ordering of the wear caused by each load case is necessary.

Let the number of load cases be K, and assume the wear due to the various load cases are arranged in ascending values of wave height. This assumption allows total service life to be calculated as demonstrated below. Once the equations developed from this assumption were programmed and a solution obtained for the total service wear, the order of the load cases was interchanged and a second solution was obtained. The two solutions agreed, showing that the ordering of the load cases does not affect the final solution.

Load case 1 is assumed to cause the first wear on the wire cross section, so the situation is exactly that considered above for constant curvature over a number of bending cycles (that is, constant δ). Equations (23) and (24) combine as before to give an equation exactly like Equation (**Error! Bookmark not defined.**) except for identifying subscripts:

$$\gamma N_1\hat{\delta}_1 I(\hat{t}_{f_1}) = \hat{t}_{f_1}^2\left[\cos^{-1}\sqrt{1 - \hat{t}_{f_1}^2} - \hat{t}_{f_1}\sqrt{1 - \hat{t}_{f_1}^2}\right] \tag{29}$$

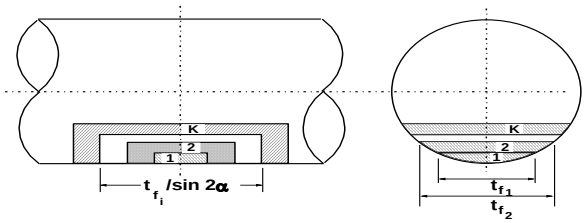

FIGURE 11 SUCCESSIVE WEAR AREAS

For the second load case, wear begins with a value of the chord equal to $\hat{t}_{f_1}$ and ends at $\hat{t}_{f_2}$ (see Figure **Error! Bookmark not defined.**). The wear area calculated by using Equation (23) is A_{w_2}, and is equal to

$$A_{w_2} = A_{seg_2} - A_{seg_1} \tag{30}$$

When this area is equated to the area given by Equation (23), and Equation (24) is used to calculate the worn area, A_{seg_2}, the result is:

$$\gamma \quad \frac{N_2 \hat{\delta}_2 \bar{\zeta}_2}{\hat{t}_{f_2}} + \frac{A_{seg_1}}{r^2} = \cos^{-1}\sqrt{1 - \hat{t}_{f_2}^{\,2}} - \hat{t}_{f_2}\sqrt{1 - \hat{t}_{f_2}^{\,2}} \tag{31}$$

where now

$$\bar{\zeta}_2 = \frac{1}{\hat{t}_{f_2} - \hat{t}_{f_1}} \int_{\hat{t}_{f_1}}^{\hat{t}_{f_2}} \zeta\left(\hat{\delta}_2\right) d\hat{t} \tag{32}$$

The dependence of ζ on the value of $\hat{\delta}_2$ has been indicated here by writing $\zeta\left(\hat{\delta}_2\right)$. Consideration of succeeding load cases leads to the following equation which applies in general for any load case, i:

$$\gamma \quad \frac{N_i \hat{\delta}_i \bar{\zeta}_i}{\hat{t}_{f_i}} + \frac{A_{seg_{i-1}}}{r^2} = \cos^{-1}\sqrt{1 - \hat{t}_{f_i}^{\,2}} - \hat{t}_{f_i}\sqrt{1 - \hat{t}_{f_i}^{\,2}} \tag{33}$$

where

$$\frac{A_{seg_{i-1}}}{r^2} = \cos^{-1}\sqrt{1 - \hat{t}_{f_{i-1}}^{\,2}} - \hat{t}_{f_{i-1}}\sqrt{1 - \hat{t}_{f_{i-1}}^{\,2}} \tag{34}$$

and

$$\bar{\zeta}_i = \frac{1}{\hat{t}_{f_i} - \hat{t}_{f_{i-1}}} \int_{\hat{t}_{f_{i-1}}}^{\hat{t}_{f_i}} \zeta\left(\hat{\delta}_i\right) d\hat{t} = \frac{1}{\hat{t}_{f_i} - \hat{t}_{f_{i-1}}} \left[\int_0^{\hat{t}_{f_i}} \zeta\left(\hat{\delta}_i\right) d\hat{t} - \int_0^{\hat{t}_{f_{i-1}}} \zeta\left(\hat{\delta}_i\right) d\hat{t} \right] \tag{35}$$

By using the definition in Equation 35, the average $\bar{\zeta}_i$ shown in the preceding equation becomes

$$\bar{\zeta}_i = \frac{I\left(\hat{\delta}_i, \hat{t}_{f_i}\right) - I\left(\hat{\delta}_i, \hat{t}_{f_{i-1}}\right)}{\hat{t}_{f_i} - \hat{t}_{f_{i-1}}} \tag{36}$$

Each term of the form $I\left(\hat{\delta}_i, \hat{t}_{f_i}\right)$ may be evaluated directly for a given value of $\hat{t}_{f_i}$ by using the equations shown in the Appendix.

QUALIFYING TEST

The qualifying test was done by fixing the umbilical cable ends to two supports, applying axial tension, and rocking one support in the plane of the umbilical to induce fully reversed bending cycles in the cable. Support rocking amplitude and tension for the test were chosen for the test based on results of the various finite element analyses of load cases for the installed umbilical.

The amplitude of the support rocking determined the magnitude of the cable curvature, κ. Umbilical properties and Equation (10) then allowed calculation of the maximum slip, δ. Contact pressure between the armor wire layers is calculated from Equation (9). This represents a uniform pressure over the *entire* developed surface of Figure 4. The force on any one particular Contact Area will be this pressure times the area, A_c, of the parallelogram formed by the lines representing the OD of the wires, that is, the area which would be in contact if the wires were worn half-way through. (Another way of saying this is the area when the chord t has become equal to the wire diameter d.) This parallelogram area is

$$A_c = \frac{d}{\sin 2\alpha} \cdot \frac{d}{\sin 2\alpha} \cdot \sin 2\alpha = \frac{d^2}{\sin 2\alpha} \tag{37}$$

Surface hardness of the armor wires for the umbilical under consideration was not known. Rabinowicz (1980) states that the hardness H is approximately equal to 3.2 times the material yield strength. Archard (1980) quotes a "widely used relationship" which states that the hardness H is approximately equal to 2.7 times the material yield strength. Feret et al (1986) use a value of 3 times the yield stress for the hardness in Archard's Law. Certainly, to one significant figure, a value of 3 times yield stress appears reasonable.

The other unknown physical property of the armor wire is the wear coefficient, k. Various literature on wear coefficients was consulted, but the most applicable appeared to be the results calculated by Nielsen et al. (1990) for flexible pipe tendon wires. The values given by Nielsen were based on the hardness being equal to 3 times the armor wire *ultimate* strength. This is not a large discrepancy with the previous discussion, since the yield strength of armor wires and flexible pipe tendon wires is raised to a value very near the material ultimate strength by the cold drawing process. Five of the eight values calculated were less than 16×10^{-6}; the others were greater than 2 times this value. So a rounded value of $k = 15 \times 10^{-6}$ was chosen. Numerical coefficients should always be used in the form of the equation used to define the coefficient, so the hardness in the present analysis was represented by 3 times the ultimate strength of the wires.

Equation 37 was programmed into an Excel spreadsheet, and a solution for $\hat{t}_f$ obtained using the Excel capability to iterate on a circular reference and a modified interval-halving technique. Properties of the umbilical are shown in Table 1.

For the test parameters of mean tension = 236kN, curvature $\kappa = 0.075$ m^{-1}, and 50,00 cycles, a final chord t = 0.844 mm was predicted. Converting chord distance to depth of wear, h, as shown in Figure 10, gave 0.0332 mm, or 0.0017 in.

TABLE 1 UMBILICAL PROPERTIES

Lay Angle (α)	20	deg
Armor Wire Diameter (d)	0.162	in
Young's Modulus	3.00E+04	ksi
Wear Coefficient (k)	1.50E-05	mm/mm
Number of Armor Wires	108	
Radius to Armor Layers (R)	39.115	mm
Ultimate Tensile Strength (S_u)	70	ksi
Coefficient of Friction	0.2	
Umbilical Service Life	15	yrs

Examination and measurement of the umbilical at the conclusion of the qualifying test showed depths of wear ranging from 0.0005 to 0.0011 in. Edges of the wear scars (where the ends of the chord meet the circular OD) were not sharp, but were rounded. This is an indication that twisting of the wires as the umbilical bends was also contributing to wear. (See Vinogradov and Atatekin, 1986.) Of course, none of the present analysis considers wire twist. If twist were to be included in the analysis, and the same volume of wear were predicted, the predicted depth of wear would be slightly less, bringing it into closer agreement with the measurements. Nevertheless, agreement between the present analysis and the qualifying test results is good, and errs on the conservative side.

SERVICE LIFE PREDICTIONS

In predicting whether an umbilical design is suitable for a desired service life, both wear and the effects of wear must be considered. The amount of wear is provided by the solution of Equation 37. Effects of wear are predicted following Feret et al. (1986)

Let the ultimate strength of the armor wire material be denoted by S_u and its endurance limit by S_E. Let σ_α represent any stress S_α non-dimensionalized by S_u, that is

$$\sigma_\alpha = \frac{S_\alpha}{S_u} \tag{38}$$

The Haigh diagram is as shown in Figure 12, and the equation of the Goodman Line is

$$\sigma_d = -\sigma_E \sigma_s + \sigma_E \tag{39}$$

Let the original operating point of an umbilical armor wire to be at point A with coordinates σ_{sA}, σ_{dA}. The equation of line OA is given by :

$$\sigma_d = \frac{\sigma_{dA}}{\sigma_{sA}} \sigma_s \tag{40}$$

As wear occurs, the cross-sectional area of the wire decreases. As the cross-sectional area decreases, the static and dynamic stresses increase (inversely proportionally to the remaining area) and the operating point moves along line OA toward Point B, the

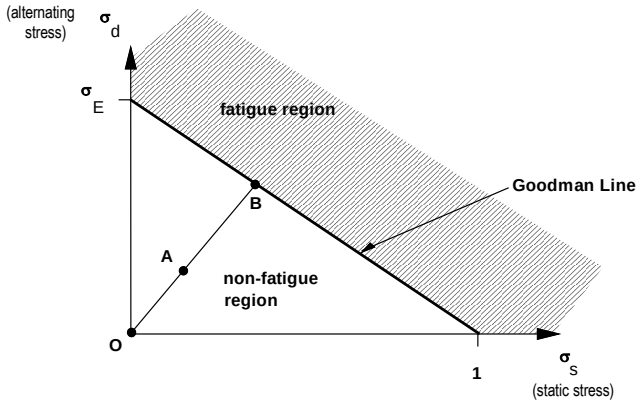

FIGURE 12 HAIGH DIAGRAM

intersection with the Goodman line. The coordinates of Point B, are obtained by simultaneous solution of Equations (39) and (40) to be

$$\sigma_{sB} = \frac{\sigma_E \sigma_{sA}}{\sigma_{dA} + \sigma_E \sigma_{sA}} \qquad \sigma_{dB} = \frac{\sigma_E \sigma_{dA}}{\sigma_{dA} + \sigma_E \sigma_{sA}} \tag{41}$$

Stress is inversely proportional to wire area, so

$$\frac{\sigma_{sB}}{\sigma_{sA}} = \frac{A_{orig}}{A_{worn}} \tag{42}$$

where A_{orig} is the original wire cross-sectional area, and A_{worn} is the cross-sectional area remaining when the operating point has reached the Goodman Line and the static stress has increased to σ_{sB}.

The worn area, A_{worn}, is the original area, A_{orig}, minus the allowable wear, A_{allow}. With this definition, Equation (42) may be solved to give

$$A_{allow} = A_{orig}\left(1 - \frac{\sigma_{sA}}{\sigma_{sB}}\right) \tag{43}$$

Wear on a sliding armor wire of radius, r, is represented by the shaded segment of the original circular cross-section as shown in Figure 10. The area of this segment is given in terms of the final chord distance t_f by Equation (24)

Once the final chord distance t_f is determined, a factor of safety based on wear area, FS, is determined to be

$$FS = \frac{A_{allow}}{A_{seg}} \tag{44}$$

where the numerator and denominator are Equations (43) and (24), respectively.

This procedure, along with the solution of Equation 37, was implemented in an Excel spreadsheet. Input data for the

calculations are as previously shown in Table 1. A portion of the spreadsheet is shown in Table 2; included are wave conditions for the various load cases, and results of the finite element analyses — mean tension, T_m, and maximum curvature in the umbilical, κ. Also shown are the calculated values of contact force, F_c, [from the product of Equations (9) and (10), curvature at which slip begins to occur [from Equation (8)], non-dimensional maximum slip, $\hat{\delta}$, [from Equation (10)], and non-dimensional chord length, $\hat{t}$ [from the solution of Equation (11)]. No wear is calculated for the lowest wave height because the maximum curvature calculated for this load case is less than the curvature which causes slip.

Because slip is assumed to be tangential as in Witz and Tan (1992) and Tan et al. (1991), Equation (7) is used for bending stress in the calculation of allowable wear, Equation (43). The value of mean tension is used in Equation (5) for the static stress. Calculated results for the dimensional value of the final chord length, t, the depth of wear, h, and the factor of safety, from Equation (44), are shown in Table 3.

The predicted (maximum) area worn from a single wire is 0.91 square mm, compared to an allowable maximum area of 8.20 square mm (at which point the wear enters the fatigue regime, see Figure 12). The safety factor against fatigue occurring is seen to be 9.0, and is hence satisfactory.

Based on the conservatism of the qualifying test wear prediction, this factor of safety should also be conservative. Additional conservatism is built in, because the condition limiting umbilical service life has been taken to be the start of fatigue, rather than fatigue failure.

CONCLUSIONS

A method of predicting wear on circular cross-section armor wires has been developed which accounts for the fact that wires are not continuously in contact during a complete bending cycle. Although based on approximate equations describing the mechanics of the helical wires and the use of average values in several critical junctures in the development, predictions of the method agreed well with results of the qualifying test.

In order to calculate service life, the method has been extended to a series of load cases, each of which produces a different value of cable curvature. However, no test results are yet available to confirm these predictions.

Tests to determine values of the wear coefficient for this specific type of wire (both geometry and material) are needed. These tests should also investigate the assumptions made about the relationship between the volume of material worn away and its distribution along the wire (Figure 9).

TABLE 3 SERVICE LIFE RESULTS

Final Chord Distance (t_f)	2.6800	mm
Total Depth of Wear (h)	0.4962	mm
Total Service Life Wear Area	0.910	mm^2
Total Allowable Wear Area	8.204	mm^2
Factor of Safety Based on Cross Section Wear Area	**9.011**	

ACKNOWLEDGMENTS

The authors wish to thank Chuck Daniels and John Evans of Multiflex, Inc. for their help and cooperation during this project, and to acknowledge Multiflex, Inc. as the source of the quoted data.

REFERENCES

Archard, J. F., 1953, "Contact and Rubbing of Flat Surfaces," *Journal of Applied Physics*, Vol. 24, pp. 981-988.

Archard, J. F., 1980, "Wear Theory and Mechanisms," *Wear Control Handbook*, M. B. Peterson and W. O. Winer, Eds., ASME, New York, NY, pp. 35-80.

TABLE 2 WEAR RESULTS BY LOAD CASE

Wave Height H (m)	Wave Period T (sec)	Annual No. of Waves N	Mean Tension T_m	Contact Force F_c (kN)	Slip Curvature (1/m)	Max Curvature κ (1/m)	Dimensionless Wire Slip $\hat{\delta}$	Dimensionless Chord $\hat{t}$
0.25	2.58	1,012,516	118.6	0.02153	0.001569	0.0011	0	0
0.75	4.90	1,724,125	118.6	0.02153	0.001569	0.0034	0.003291	0.416869
1.25	6.61	1,376,350	118.6	0.02153	0.001569	0.0057	0.005486	0.524867
1.75	7.67	762,118	118.6	0.02153	0.001569	0.0080	0.007680	0.577647
3.75	9.92	608,531	118.6	0.02153	0.001569	0.0195	0.018719	0.647479
5.25	10.87	19,326	118.6	0.02153	0.001569	0.0345	0.033119	0.650813
6.73	11.00	1,672	118.6	0.02153	0.001569	0.0475	0.045599	0.651204
8.25	12.60	233	118.6	0.02153	0.001569	0.0735	0.070558	0.651287
8.75	13.00	9	118.6	0.02153	0.001569	0.0825	0.079198	0.651291
9.25	12.00	18	118.6	0.02153	0.001569	0.0845	0.081118	0.651298
9.75	10.00	18	120.5	0.02187	0.001594	0.1070	0.102717	0.651308

Berge, S., and Olufsen, A., 1992, *Handbook on Design and Operation of Flexible Pipes*, Chapter 3, "Failure Modes and Cross Section Analysis, Report STF70A92006, SINTEF Structural Engineering, Trondheim, Norway.

Casey, N. F., and Lee, W. K., 1989, "The Fatigue Failure of Large Diameter Six Strand Wire Rope," *International Journal of Fatigue*, Vol. 11, pp. 78-84.

Chang, Y. J., and Kulhmann-Wilsdorf, D., 1987, "A Case of Wear Particle Formation Through Shearing-Off at Contact Spots Interlocked Through Microroughness in Adhesive Wear," *Wear*, Vol. 120, pp. 175-197.

Claydon, P., Cook, G., Brown, P. A., and Chandwani, R., 1992, "A Theoretical Approach to Prediction of Service Life of Unbonded Flexible Pipes under Dynamic Loading Conditions," Marine Structures, Vol. 5, pp. 399-429.

Estrier, P. 1992, "Updated Methods for the Determination of the Service Life of Flexible Risers," *MARINFLEX 92, Flexible Pipes, Umbilicals, Marine Cables, Proc. First European Conference*, J. A. Witz and M. H. Patel, Eds., BPP Technical Services, London.

Feret, J. J., Bournazel, C. L., and Rigaud, J., 1986, "Evaluation of Flexible Pipes' Life Expectancy Under Dynamic Conditions," *Proc. 18th Annual Offshore Technology Conference*, Vol. 3, pp. 83-90.

Feret, J. J., and Bournazel, C. L. 1987, "Calculation of Stresses and Slip in Structural Layers of Unbonded Flexible Pipes," *Journal of Offshore Mechanics and Arctic Engineering*, Vol. 109, pp. 263-269.

Knapp, R. H., and Chiu, E. Y. C., 1988, "Tension Fatigue Model for Helically Armored Cables", *Journal of Energy Resources Technology*, Vol. 110, pp. 12-18.

Llorca, J., Varona, J. M., Sanchea-Galvez, V., and Gutierrez Solana, F., 1989, "Fatigue Behavior of Wire Ropes," Materials and Structures, Vol. 22, pp. 411-419.

Nielsen, R., Colquhoun, R. S., McCone, A., Witz, J. A., and Chandwani, R.., 1990, "Tools for Predicting Service Life of Dynamic Flexible Risers," *Proc. First European Offshore Mechanics Symposium*, Trondheim, Norway, pp. 449-456.

Rabinowicz, E., 1980, "Wear-Coefficients - Metals," *Wear Control Handbook*, M. B. Peterson and W. O. Winer, Eds., ASME, New York, NY, pp. 475-506.

Raoof, M., 1993, "Design of Steel Cables Against Free-Bending Fatigue at Terminations," The Structural Engineer, Vol. 71, pp. 171-178.

Tan, Z, Witz, J. A., Lyons, G. J., Fang, J., and Patel, M. H., 1991, "On the Influence of Internal Slip Between Component Layers on the Dynamic Response of Unbonded Flexible Pipe," *Proc. 10th International Conference on Offshore Mechanics and Arctic Engineering*, Vol. I-B, pp. 563-569.

Velinsky, S. A., and Schmidt, J. D., 1988, "A Simplified Treatise on the Effect of Wear in Cables," *Journal of Offshore Mechanics and Arctic Engineering*, Vol. 110, pp. 32-37.

Vinogradov, O. G., and Atatekin, I. S., 1986, "Internal Friction Due to Wire Twist in Bent Cable," *Journal of Engineering Mechanics*, Vol. 112, pp. 859-873.

Witz, J. A., and Tan, Z., 1992, "Structural Mechanics of Marine Cables and Umbilicals in Rotary Bending Testing Rigs," *MARINFLEX 92, Flexible Pipes, Umbilicals, Marine Cables, Proc. First European Conference*, J. A. Witz and M. H. Patel, Eds. BPP Technical Services, London.

APPENDIX - EVALUATION OF INTEGRALS

The integrals defined by Equation (45) for each region of ζ are evaluated using Equations (46) - (47). From the first of these

$$0 \le \hat{t}_f < \hat{\delta} \sin 2\alpha$$

$$I(\hat{t}_f) = \int_0^{\hat{t}_f} \frac{\hat{t}}{2\hat{\delta} \sin 2\alpha} d\hat{t} = \frac{\hat{t}_f^2}{4\hat{\delta} \sin 2\alpha} \tag{45}$$

In the second region, the integral must be evaluated by integrating over the complete first region with its associated formula for ζ, and then continuing into the second region with its associated formula for ζ, thus

$$\hat{\delta} \sin 2\alpha \le \hat{t} < 2\hat{\delta} \sin 2\alpha$$

$$\begin{aligned} I(\hat{t}_f) &= \int_0^{\hat{\delta} \sin 2\alpha} \frac{\hat{t}}{2\hat{\delta} \sin 2\alpha} d\hat{t} + \frac{1}{4} \int_{\hat{\delta} \sin 2\alpha}^{\hat{t}_f} \left[1 + \frac{\hat{t}}{\hat{\delta} \sin 2\alpha} \right] d\hat{t} \\ &= \frac{1}{4} \left[\hat{t}_f + \frac{\hat{t}_f^2}{2\hat{\delta} \sin 2\alpha} - \frac{1}{2} \hat{\delta} \sin 2\alpha \right] \end{aligned} \tag{46}$$

Similarly, in the third region,

$$2\hat{\delta} \sin 2\alpha \le \hat{t} < 1 - \hat{\delta} \sin 2\alpha$$

$$\begin{aligned} I(\hat{t}_f) &= \int_0^{\hat{\delta} \sin 2\alpha} \frac{\hat{t}}{2\hat{\delta} \sin 2\alpha} d\hat{t} + \frac{1}{4} \int_{\hat{\delta} \sin 2\alpha}^{2\hat{\delta} \sin 2\alpha} \left[1 + \frac{\hat{t}}{\hat{\delta} \sin 2\alpha} \right] d\hat{t} \\ &\quad + \int_{2\hat{\delta} \sin 2\alpha}^{\hat{t}_f} \left[1 - \frac{\hat{\delta} \sin 2\alpha}{2\hat{t}} \right] d\hat{t} \\ &= \hat{t}_f - \frac{1}{2} \hat{\delta} \sin 2\alpha \ \ln \left(\frac{\hat{t}_f}{2\hat{\delta} \sin 2\alpha} \right) - \frac{9}{8} \hat{\delta} \sin 2\alpha \end{aligned} \tag{47}$$

and in the fourth region,

$$1-\hat{\delta}\ \sin 2\alpha\ \le\ \hat{t}\le 1$$

$$\begin{aligned} I(\hat{t}_f) = & \int_0^{\hat{\delta}\sin 2\alpha} \frac{\hat{t}}{2\hat{\delta}\ \sin 2\alpha}\, d\hat{t} + \frac{1}{4}\int_{\hat{\delta}\sin 2\alpha}^{2\hat{\delta}\sin 2\alpha}\left[1+\frac{\hat{t}}{\hat{\delta}\ \sin 2\alpha}\right] d\hat{t} \\ & + \int_{2\hat{\delta}\sin 2\alpha}^{1-\hat{\delta}\sin 2\alpha}\left[1-\frac{\hat{\delta}\ \sin 2\alpha}{2\hat{t}}\right] d\hat{t} + \int_{1-\hat{\delta}\sin 2\alpha}^{\hat{t}_f}\left[1-\frac{1-\hat{t}}{2\hat{t}}\right] d\hat{t} \qquad (48) \\ = & \frac{3}{2}\hat{t}_f - \frac{1}{2}\ln\left(\hat{t}_f\right) - \frac{1}{2} + \frac{1}{2}\left(1-\hat{\delta}\ \sin 2\alpha\right)\ \ln\left(1-\hat{\delta}\ \sin 2\alpha\right) \\ & + \frac{1}{2}\hat{\delta}\sin 2\alpha\ \ln\left(2\hat{\delta}\ \sin 2\alpha\right) - \frac{5}{8}\hat{\delta}\ \sin 2\alpha \end{aligned}$$